Black-Box Modeling Approach for Evaluating Internal Resonances in High-Voltage Windings

Felipe Luis Probst, Michael Beltle, Mauricio Valencia Ferreira da Luz, Stefan Tenbohlen

Abstract-- **This paper presents a black-box modeling approach for evaluating internal resonances in high-voltage windings of power transformers. The proposed method relies on frequency response measurements, specifically admittance and voltage transfer functions, over a frequency range of 20 Hz to 1 MHz. First, the black-box modeling methodology is presented, followed by a discussion of the frequency response measurements performed in a high-voltage laboratory environment using a Sweep Frequency Response Analysis (sFRA) instrument. Based on these measurements, Y-matrix and H-matrix models were developed and validated in both frequency and time domains. The analysis revealed critical resonance frequencies, especially the first-mode resonance, which cause significant overvoltages that pose a risk to the integrity of the winding's insulation. These results highlight the importance of considering internal resonances during the design phase of power transformers to mitigate the risk of dielectric failure. Furthermore, the technique proves especially valuable for post-failure analysis, as it enables the investigation of resonance frequencies in a failed transformer or similarly designed unit, providing insight into whether these resonances contributed to the failure event in the operational power grid.**

Keywords: **Black-Box Model, Frequency Response, High-Voltage Winding, Internal Resonance, Power Transformer, Voltage Transfer.**

I. Introduction

POWER transformers are exposed to various electromagnetic transients, such as energization overvoltages, lightning strikes, and switching operations, which can lead to dielectric failures. These transients may arise from external events or interactions between the transformer and the connected power system [1]. Given the critical nature of these interactions, many technical standards and guidelines have been developed to address the associated risks [1]-[8]. These documents provide comprehensive case studies and propose strategies to mitigate the risk of transformer failures.

One particularly concerning condition is resonance within the transformer winding, also known as internal resonance. When a switching event or other transient aligns with one of the transformer's natural frequencies, it may excite an internal resonance, generating voltages significantly above the rated level, even when the voltage at the transformer terminals remains within specification limits [1]. Accurately investigating these internal resonances requires a detailed and precise model of the high-voltage winding. This ensures that the winding's behavior under transient conditions is properly represented and potential resonances are identified.

Several studies have focused on modeling transformer windings to analyze internal overvoltages [9]-[15]. However, most approaches rely on detailed winding geometry or comprehensive white-box models, which are typically proprietary and held by manufacturers. This restricts the practical use of such models in independent studies where detailed design data is often unavailable.

To address this limitation, this paper presents a black-box model of the high-voltage winding of a distribution transformer to investigate internal resonances. The model is based on measurements of admittance and voltage transfer functions over a frequency range of 20 Hz to 1 MHz, conducted in a high-voltage laboratory using a Sweep Frequency Response Analysis (sFRA) instrument. This approach is particularly valuable for transformer failure analysis, as it allows the development of a detailed model without requiring information about the winding geometry.

This paper outlines the methodology to develop a black-box model based on frequency response measurements, validates the model in both frequency and time domains, and analyzes the measurement results. Section II details the black-box modeling technique based on admittance and voltage transfer functions. Section III describes the key characteristics of the winding under investigation. Section IV presents the frequency response measurements used to construct the model. Sections V and VI discuss the development and validation of the model. Section VII examines the internal resonances identified in the high-voltage winding and their potential effects. Finally, Section VIII addresses specific points related to the implementation of the methodology, while Section IX presents the conclusions of the study.

II. Black-Box Model Based on Admittance and Voltage Transfer Function Measurements

Black-box models are widely employed for broadband modeling of power transformers [16]-[20]. Unlike the white-box, which requires detailed knowledge of a transformer's internal geometry, black-box models represent the equipment behavior using rational functions or equivalent circuits derived from frequency response measurements. This method simplifies the modeling process while maintaining high accuracy across a wide frequency range, making it particularly effective for fast transient analysis and system-level studies.

F. L. Probst, M. Beltle and S. Tenbohlen are with the Institute of Power Transmission and High Voltage Technology (IEH), University of Stuttgart, 70569 Stuttgart, Germany (email: felipe-luis.probst@ieh.uni-stuttgart.de; michael.beltle@ieh.uni-stuttgart.de; stefan.tenbohlen@ieh.uni-stuttgart.de).
M. V. Ferreira da Luz is with the Department of Electrical and Electronic Engineering, Federal University of Santa Catarina (UFSC), CEP 88040-900, Florianópolis, Brazil (email: mauricio.luz@ufsc.br).

Paper submitted to the International Conference on Power Systems Transients (IPST2025) in Guadalajara, Mexico, June 8-12, 2025.

The approximation of frequency response measurements into rational functions is typically done using the vector fitting method [21]. This approach is applicable to various parameter types, including admittance, impedance, scattering parameters, and voltage transfer functions. In this study, it is applied to admittance and voltage transfer functions. The admittance matrix **Y** establishes the relationship between the terminal voltages and currents over the measured frequency range. Meanwhile, the voltage transfer, represented by the **H** matrix, quantifies the voltage at a designated set of nodes in response to a known input voltage applied at an external terminal [16].

The black-box model derived from the **Y** matrix can be converted into an equivalent circuit for time-domain simulation using EMTP-type programs [22]. The **Y** matrix must be square and symmetrical, with the number of rows and columns corresponding to the number of terminals modeled. For example, if a winding is represented by one external terminal and nine internal terminals, the **Y** matrix will have a dimension of 10 x 10, requiring 100 frequency response measurements. This is necessary when all terminals interact with the circuit, such as when loads or voltage limiters are connected to internal terminals.

However, if the interaction between the internal terminals and external circuits is outside the scope of the application, as is the case in this work, the H-matrix model becomes more efficient. Unlike the **Y** matrix, which models the full interaction between all terminals, the **H** matrix focuses solely on the response of the internal terminals to the external voltage, excluding feedback to external circuits. Referring to the previous example, the **H** matrix would be a 9 x 1 matrix, representing the voltages at the internal terminals for a known voltage applied to the external terminal. This approach reduces the number of frequency response measurements to just 10: one for admittance and nine for voltage transfers. Therefore, the black-box model implemented in this study integrates both Y-matrix and H-matrix models, as outlined in Fig. 1.

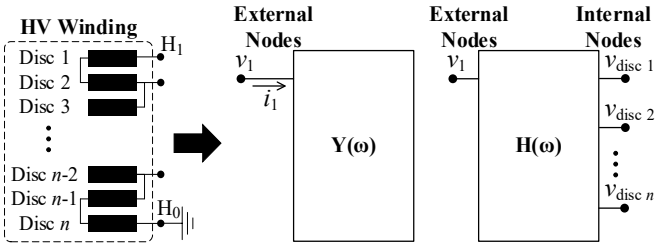

Fig. 1. Black-box model of a high-voltage winding using Y and H matrices.

The Y-matrix model must be stable, passive, and symmetrical, while the H-matrix model requires only stability [16]. The passivity of the Y-matrix model is ensured through a post-processing step that assesses and enforces passivity [23]. Once passivity is enforced, the Y-matrix model can be transformed into an equivalent circuit and implemented in an EMTP-type program (ATPDraw in this work) for time-domain simulation. In contrast, since the H-matrix model does not interact with external circuits, it is not converted into an equivalent circuit. Instead, the response of the linear system is evaluated in time domain converting the linear model from frequency to time domain. Fig. 2 illustrates the modeling flowchart, detailing the process from measurements to time-domain simulation for both Y-matrix and H-matrix models.

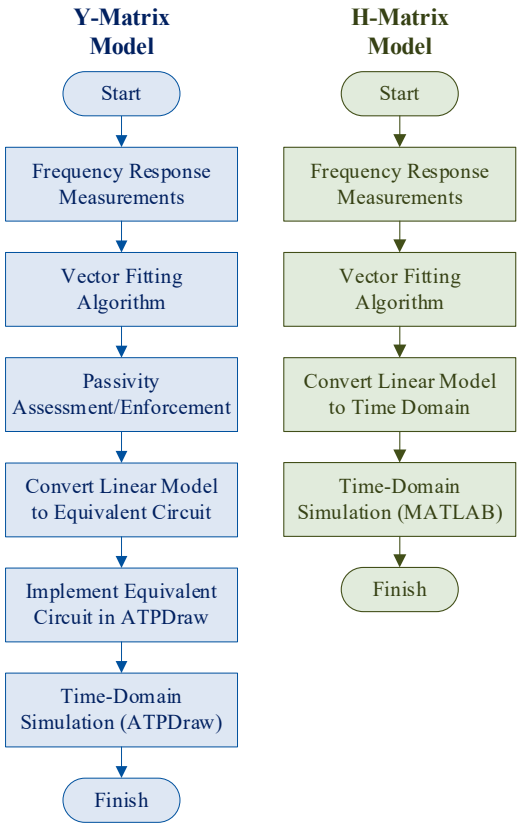

Fig. 2. Flowcharts outlining the modeling process for Y and H matrices.

III. Characteristics of the High-Voltage Winding Under Investigation

This section provides an overview of the high-voltage winding selected for testing and modeling. The winding, originated from a 1 MVA oil-filled distribution transformer, features a continuous disc design and a rated voltage of 10 kV. Key specifications are summarized in Table I.

TABLE I
PARAMETERS OF THE HIGH-VOLTAGE WINDING

Parameter	Specification
Number of discs	60
Turns per disc	11
Winding height	865 mm
Winding inner radius	147.5 mm
Metallic cylinder radius	105 mm
Winding insulation	Oil-impregnated paper

A hollow metallic cylinder inside the winding provides a ground reference, analogous to the transformer's iron core. Additionally, each even-numbered disc has a terminal, enabling the measurement of internal voltages and, consequently, voltage transfer functions. Fig. 3 presents a schematic diagram and an image of the high-voltage winding under test, highlighting the internal connections.

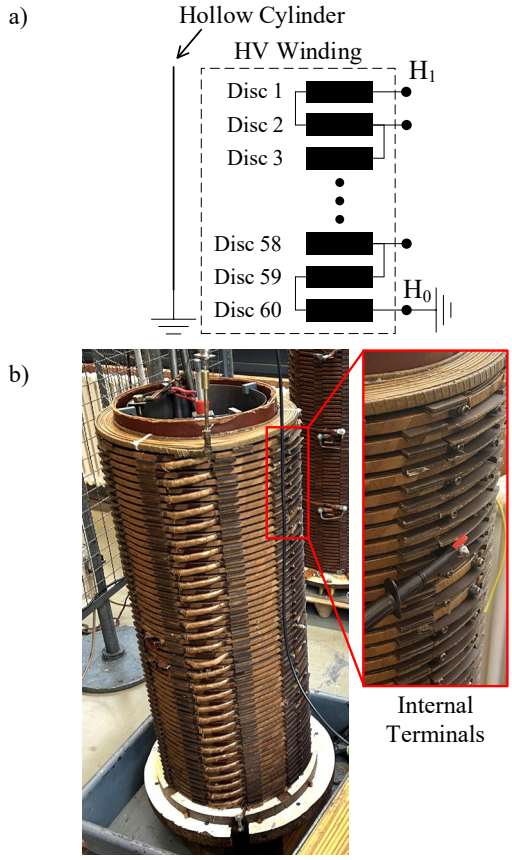

Fig. 3. High-voltage winding. (a) Schematic diagram. (b) Details of internal terminals.

IV. Frequency Response Measurements

As outlined in Section II, the black-box model developed in this study relies on admittance and voltage transfer functions. Accordingly, frequency response measurements of the winding were performed in two configurations to obtain the **Y** and **H** matrices. Using an sFRA instrument, these measurements spanned a frequency range of 20 Hz to 1 MHz.

The sFRA instrument (Omicron FRAnalyzer) has three primary connections: the output channel, which provides the generated sinusoidal voltage; channel 1, used to measure the reference voltage; and channel 2, used to measure the voltage of interest. The device operates in two modes: gain mode, which measures the voltage transfer between channels 1 and 2, and impedance/admittance mode, where the circuit impedance or admittance is measured through the output channel. Fig. 4 shows the setup used to measure the winding admittance.

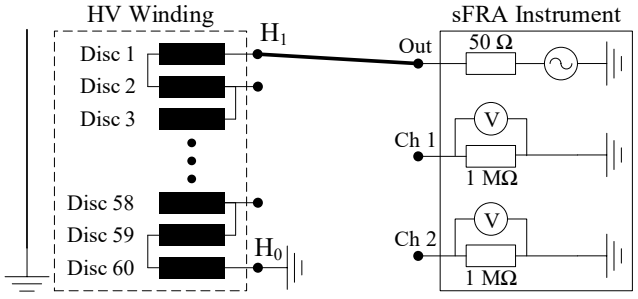

Fig. 4. Test setup for measuring the winding admittance.

In this configuration, the sFRA instrument operates in impedance/admittance mode to measure the admittance between terminals H_1 and H_0. The output channel of the sFRA instrument is connected to terminal H_1 through a 1 m coaxial cable with a grounded shield. The winding admittance is calculated in the frequency domain according to (1).

$$Y_{11}(\omega) = \frac{i_1(\omega)}{v_1(\omega)} \tag{1}$$

where ω is the angular frequency, v_1 is the applied voltage, and i_1 is the current flowing through the winding, measured directly by the instrument through its 50 Ω output impedance.

Terminal H_0 is grounded, the same condition in which the voltage transfers are measured. Consequently, terminal H_1 is the only external terminal considered in the model, resulting in a **Y** matrix with only one element. Fig. 5 shows the measured winding admittance.

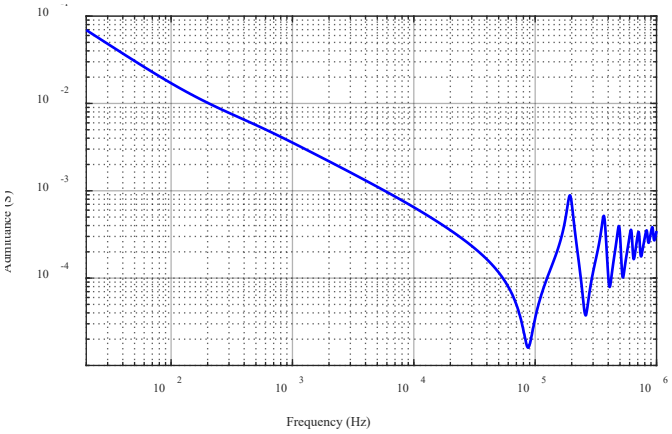

Fig. 5. Winding admittance in the frequency domain.

The admittance exhibits a series of resonances and anti-resonances, where resonances correspond to points of high admittance (or low impedance) and anti-resonances indicate points of low admittance. In this context, resonances represent internal voltage maxima, while anti-resonances correspond to internal voltage minima [8]. Given this understanding, the study focuses on evaluating resonance frequencies to investigate internal overvoltages. The first three resonance modes are observed at frequencies of 190 kHz, 367 kHz, and 488 kHz, respectively.

Subsequently, the voltage transfer functions were measured using the setup illustrated in Fig. 6.

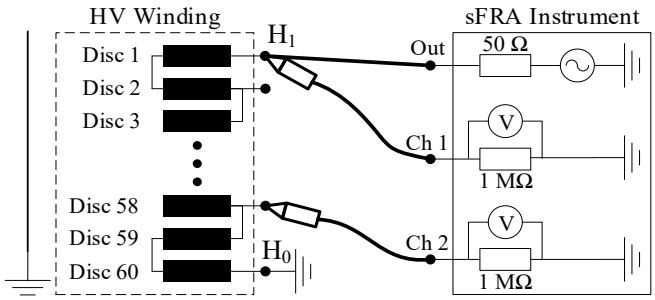

Fig. 6. Test setup for measuring the voltage transfer functions.

The sFRA instrument operates in gain mode to measure the voltage transfer function between the winding's internal nodes and terminal H_1, while terminal H_0 is grounded. The output channel and channel 1 are connected to terminal H_1 to apply and measure the voltage, respectively. Channel 2 is connected to the internal node of interest to calculate the transfer function. To prevent the shunt capacitance of measurement cables from loading the winding and affecting the internal node voltage, both voltages are measured using a 10:1 passive voltage probe (Lecroy PP005), as proposed in [16]. This setup enables an accurate calculation of the voltage transfer function at internal node *j* according to (2).

$$H_j(\omega) = \frac{v_j(\omega)}{v_1(\omega)} \tag{2}$$

where v_1 is the applied voltage measured by channel 1 and v_j is the voltage measured at node *j* by channel 2.

The voltage transfer functions for all even-numbered discs, from 2 to 58, were measured across a frequency range of 20 Hz to 1 MHz. Consequently, the resulting **H** matrix contains 29 rows and a single column. Fig. 7 presents the measurement results for discs 14, 30, and 46.

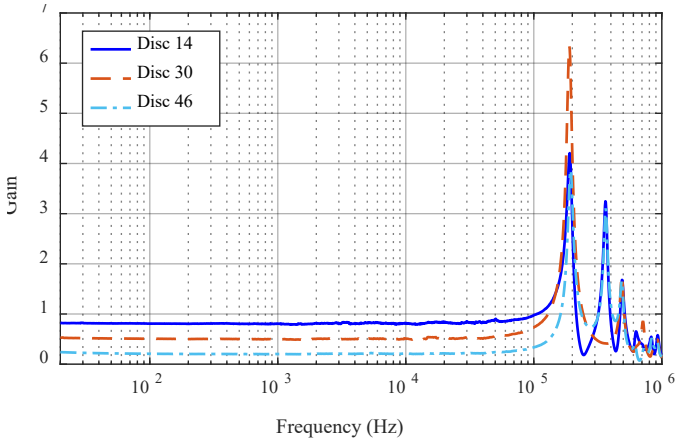

Fig. 7. Voltage transfer functions of discs 14, 30 and 46.

Discs 14 and 46 are positioned at approximately 75% and 25% of the winding height, respectively, while disc 30 is located at the midpoint. The gain remains constant from 20 Hz to approximately 50 kHz, consistent with the operational gain at 50 Hz. The resonance frequencies correspond to those observed at the winding terminal. However, disc 30 does not exhibit a resonance at 367 kHz. This absence is expected, as 367 kHz corresponds to the second-mode resonance, characterized by amplitude maxima at 25% and 75% of the winding height and zero amplitude at the midpoint.

At the first-mode resonance, the maximum voltage is expected at the midpoint of the winding. At this frequency, the measured maximum gain reaches approximately 6.3, indicating that an input voltage at 190 kHz applied to terminal H_1 results in a midpoint voltage 6.3 times higher, which significantly exceeds the design specifications of the winding insulation. Fig. 8 shows the voltage transfer functions along the winding. Since the response is flat at low frequencies, the results are shown starting from 50 kHz.

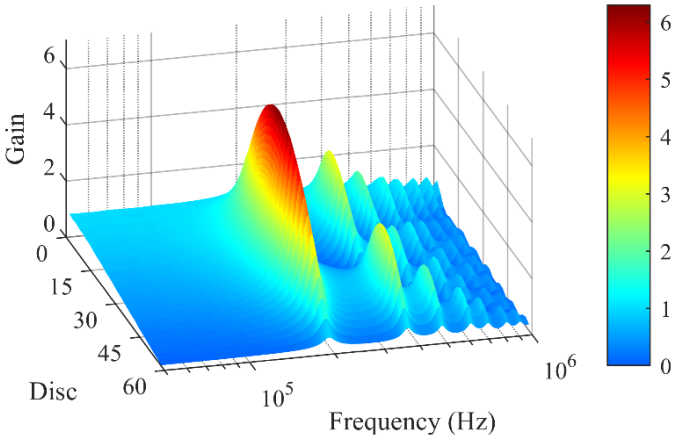

Fig. 8. Voltage transfer functions along the winding.

The graph in Fig. 8 exhibits the resonance modes until 1 MHz. The first-mode resonance at 190 kHz shows a maximum at disc 30 (winding midpoint). The second-mode resonance at 367 kHz exhibits two maxima at discs 14 and 46. The third-mode resonance at 488 kHz has three maxima at discs 10, 30, and 50. Higher-order resonance modes are also evident, with each mode showing a number of maxima corresponding to its order. A more detailed analysis of the winding's internal resonances is provided in Section VII.

V. Modeling

Based on the frequency response measurements presented in Section IV, the winding model is developed in both frequency and time domains.

A. Y-Matrix Model

To construct the Y-matrix model, the admittance measurement is subjected to a rational approximation with 25 poles using the vector fitting algorithm [21]. The selection of 25 poles is based on a balance between model accuracy and the complexity of the equivalent circuit implemented in ATPDraw, as overly complex circuits may lead to numerical instability. Fig. 9 compares the measured winding admittance with the model's response.

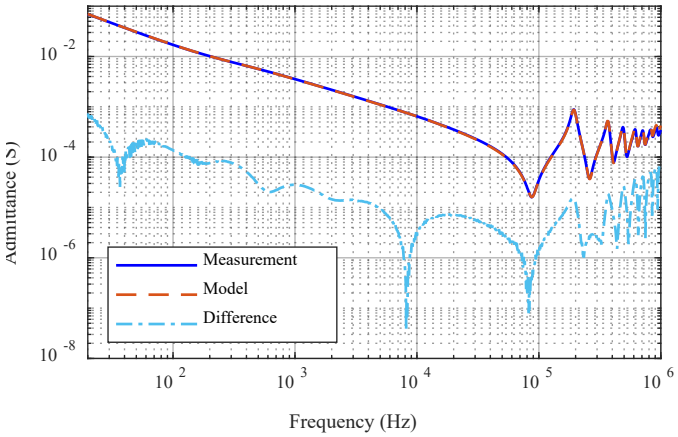

Fig. 9. Comparison of winding admittance between measured data and the rational approximation model.

The model demonstrates good agreement with the measurements, as indicated by the difference curve in Fig. 9. Following the vector fitting process, the model underwent a passivity assessment. No passivity violations were detected, indicating that passivity enforcement was not necessary.

B. Time-Domain ATP Model

For time-domain simulation in an Electromagnetic Transients Program (EMTP), the linear model is converted into an equivalent circuit represented by a complex RLCG network. This transformation is achieved using a MATLAB routine provided in the vector fitting toolbox [22], which generates a data file to import into ATPDraw. Fig. 10 illustrates the equivalent circuit as implemented in ATPDraw.

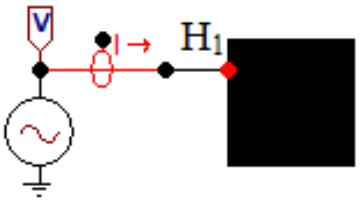

Fig. 10. Black-box model implemented in ATPDraw.

The equivalent circuit is encapsulated within the black box, with terminal H_0 internally grounded. Terminal H_1 is the only external terminal. In this example, a sinusoidal voltage source is connected to the winding model, and both the applied voltage and resulting current are measured. Since the model interacts with external circuits, it can be used in various time-domain studies, such as evaluating transformer winding interactions with high-voltage cables during vacuum circuit breaker switching events.

To validate the ATP model in the frequency domain, the admittances of both the MATLAB and ATP models are compared over the frequency range of 20 Hz to 1 MHz, as shown in Fig. 11. The responses are identical, indicating that the ATP model accurately represents the MATLAB model and, consequently, the real winding.

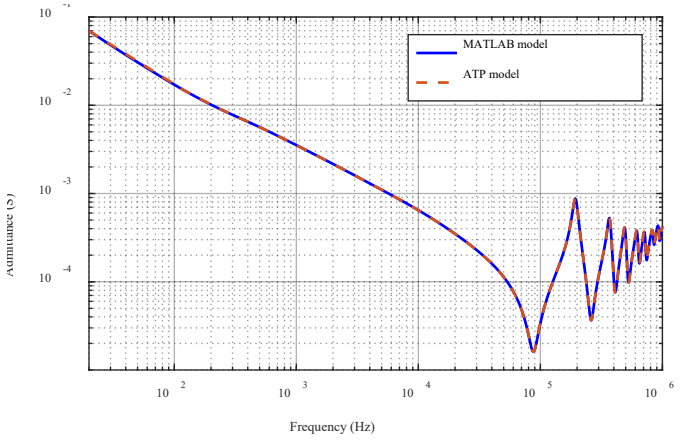

Fig. 11. Comparison of winding admittance between MATLAB and ATP models.

C. H-Matrix Model

The second component of the proposed modeling technique is the H-matrix model. In this approach, the measured voltage transfer functions are approximated using a rational function through a curve-fitting process. The model is constructed using the vector fitting algorithm with 250 poles, chosen to minimize approximation error and improve accuracy. Although a high number of poles increases the model's complexity, it does not introduce instability, as occurs when the model is converted into an equivalent circuit. Fig. 12 shows a comparison between the measured voltage transfer functions and the model's response for discs 14 and 30.

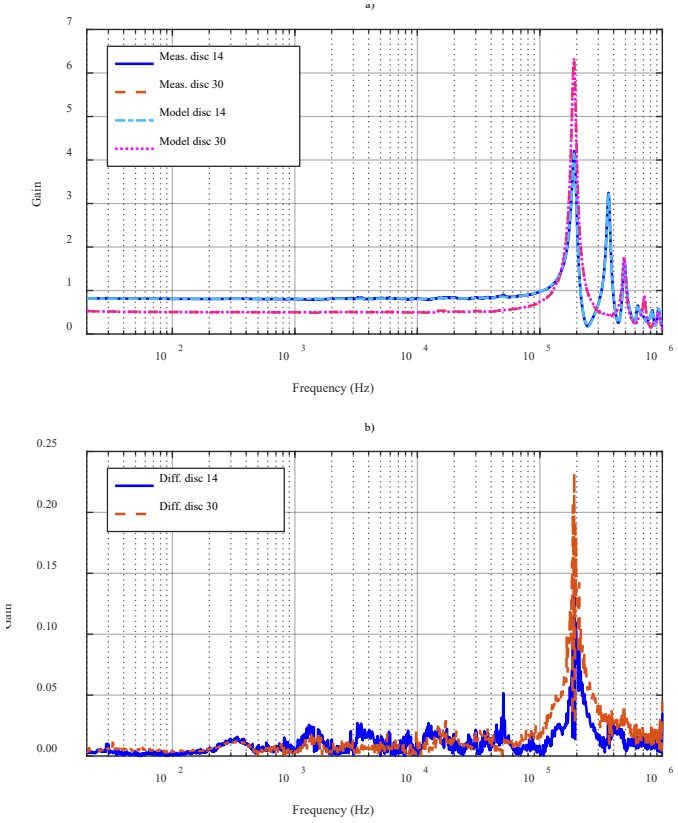

Fig. 12. Comparison of winding voltage transfer functions for discs 14 and 30. (a) Measurement vs. model. (b) Difference.

The H-matrix model exhibits good correlation with the measurements, as evidenced by the difference curves shown in Fig. 12. As detailed in Section II, this model does not require passivity enforcement. Furthermore, it is not converted into an equivalent circuit because it does not interact with external circuits. The time-domain simulation is performed in MATLAB, where the rational function is converted from frequency to time domain.

The modeling of the **Y** and **H** matrices is conducted separately, but they are integrated for evaluating resonances within the transformer winding. First, a time-domain simulation is executed in ATPDraw, based on the relevant topology and specific study objectives. Then, the voltage at terminal H_1 is recorded and used as input to the H-matrix model to calculate internal overvoltages across the winding.

VI. Model Validation in Time Domain

After implementing the model, validation in time domain is conducted by comparing its response to measured values. A signal generator is used to apply the voltage to the winding, with the input voltage and voltage at disc 30 measured using 10:1 passive voltage probes. The input current is measured with a TESTEC TT-CC 550 current probe (200 mA/V). All probes are connected to a RIGOL DS1074 oscilloscope, where measurements are recorded.

The first signal applied to the winding is a nonstandard impulse with a rise time of 100 µs and a decay time of 900 µs. Fig. 13 compares the model's voltage and current responses with the measurement results.

The model's predicted voltage and current closely match the voltage measured at disc 30 and the current measured at the input terminal. The observed current differences fall within the current probe's accuracy of ±3%. Further validation was performed by applying a 190 kHz sinusoidal voltage (first-mode resonance), resulting in model responses that also closely align with measured values.

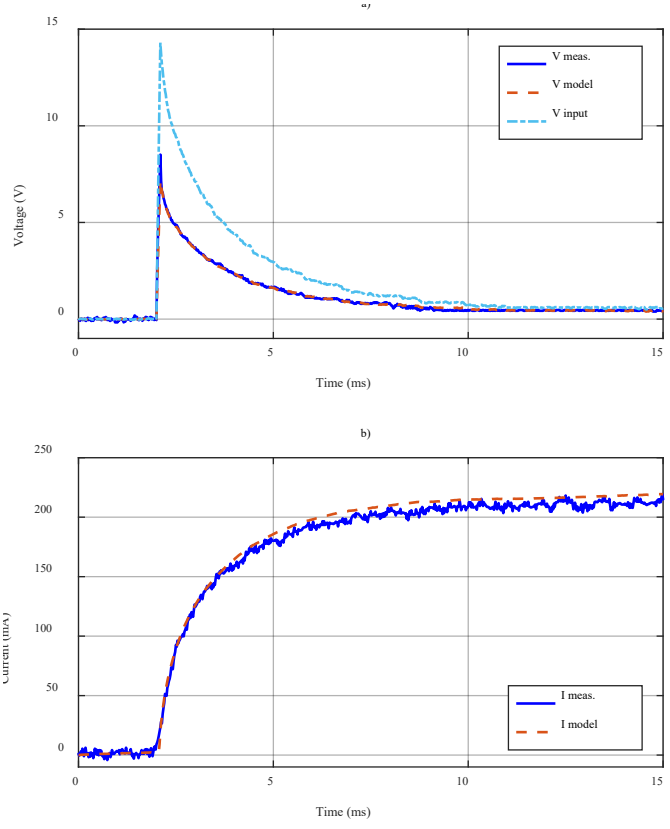

Fig. 13. Time-domain response to an impulse. (a) Voltage. (b) Current.

Once validated, the model is ready for application in diverse transient studies. However, this is beyond the scope of the current work and is not explored here.

VII. Evaluation of Internal Resonances

The frequency response measurements presented in Section IV indicate that the first-mode resonance results in an overvoltage of 6.3 times the applied input voltage. Using the developed model, the voltage distribution along the winding can be accurately analyzed when the maximum overvoltage occurs at the winding's midpoint. Moreover, this methodology can be extended to evaluate voltage profiles for higher-order resonance modes. Fig. 14 shows the voltage distribution along the winding for the first three resonance modes, obtained from the model with an assumed input voltage of 1 p.u.

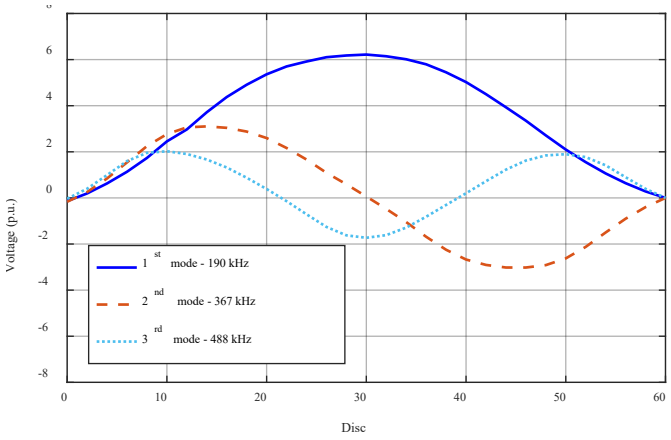

Fig. 14. Voltage distribution along the winding for three resonance modes.

The first-mode resonance exhibits a maximum overvoltage of 6.2 p.u. at disc 30, corresponding to the winding's midpoint. This result, derived from the developed model, closely aligns with the frequency response measurement outcomes. An overvoltage of this magnitude poses a significant risk to the winding insulation and may lead to dielectric failure between the winding and ground. The second-mode resonance produces two maximum overvoltages of 3.1 and -3.0 p.u. at discs 14 and 46, respectively, which also present a significant risk of dielectric failure. Similarly, the third-mode resonance results in three maximum overvoltages of 2.0, -1.7, and 1.9 p.u. at discs 10, 30, and 50, respectively.

In addition to the potential failure between the winding and ground, failures may also occur between adjacent discs if the voltage difference exceeds the insulation design limits. Fig. 15 presents the voltage differences between adjacent discs, where the maximum voltage difference for each disc is calculated relative to its preceding disc.

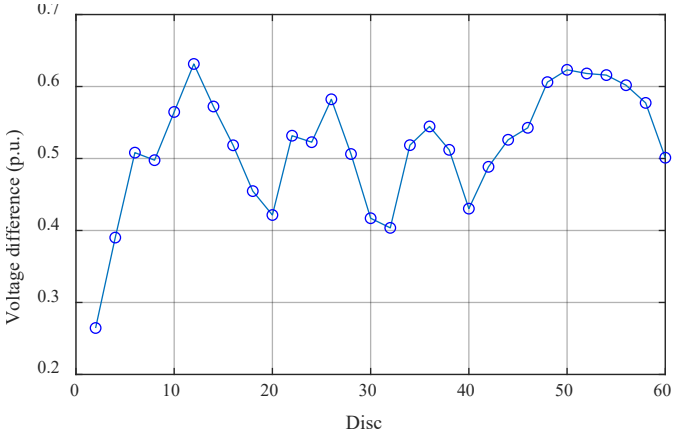

Fig. 15. Maximum voltage difference between adjacent discs.

The highest voltage differences are observed between discs 12 and 10 (0.63 p.u.) and discs 50 and 48 (0.62 p.u.), both occurring at the first-mode resonance frequency. If the insulation between discs is not rated for these voltage differences, dielectric failure may occur.

The results suggest that mitigation measures, such as RC snubbers or varistors, are necessary to reduce the risk of failure if the evaluated winding were in operation. However, installing these components only at the winding terminals may not be sufficient to mitigate internal resonances. As an alternative, placing varistors between intermediate points in the winding could provide a more effective solution.

VIII. Discussion

The methodology presented in this work was applied to a high-voltage winding not integrated into a transformer but can also be extended to windings installed in transformers. The primary differences are expected to arise from the influence of the low-voltage winding, the insulation medium (e.g., oil or epoxy resin), and the transformer tank (if oil-filled), as these factors affect the capacitances and, consequently, the resonance frequencies. Additionally, the transformer iron core impacts the frequency response below 100 kHz [24], with its effect also dependent on the voltage level applied during measurements [25]. However, since the resonance frequencies of interest are above 100 kHz, the iron core is not expected to influence the evaluation of internal resonances.

Moreover, the discussed technique requires direct access to the winding discs. For oil-filled transformers, this entails removing the active part from the tank, while for dry-type transformers, partial removal of the epoxy insulation is necessary to expose the high-voltage winding discs. Therefore, this approach is particularly valuable for post-failure analysis, enabling its application to a failed transformer or a similarly designed unit to investigate resonance frequencies and evaluate their role in the failure event in the power grid.

IX. Conclusions

Transient events, such as switching operations, can excite internal resonances within a transformer when their frequencies align with the transformer's natural frequencies. This effect can result in voltage amplification beyond rated levels, posing a significant risk to the equipment. Therefore, precise modeling of the high-voltage winding is crucial for accurately analyzing and understanding these internal resonances.

This study introduced a black-box modeling approach for evaluating internal resonances in high-voltage windings of power transformers. The methodology, based on frequency response measurements, provides a detailed representation of the winding's dynamic behavior without requiring proprietary design details.

The modeling process involved the development of Y-matrix and H-matrix models, which were validated in both frequency and time domains. The analysis identified critical resonance frequencies, particularly the first-mode resonance, showing significant overvoltages capable of compromising the winding's insulation system.

The findings underscore the importance of addressing internal resonances during the transformer design phase to mitigate the risk of dielectric failure. Additionally, the technique can be applied to model high-voltage windings within power transformers, though some variation in resonance frequencies may occur due to the presence of the low-voltage winding and insulation media. As the approach requires direct access to the winding discs, it is particularly well-suited for post-failure investigations, enabling the assessment of resonance frequencies and their potential role in transformer failures.

X. References

[1] CIGRE TB 577A, "Electrical transient interaction between transformers and the power system - Part 1: Expertise", JWG A2/C4.39, 2014.

[2] CIGRE TB 577B, "Electrical transient interaction between transformers and the power system - Part 2: Case studies", JWG A2/C4.39, 2014.

[3] CIGRE TB 939, "Analysis of AC transformer reliability", WG A2.62, 2024.

[4] CIGRE TB 881, "Electromagnetic transient simulation models for large-scale system impact studies in power systems having a high penetration of inverter-connected generation", WG C4.56, 2022.

[5] IEC 60071-1, "Insulation co-ordination - Part 1: Definitions, principles and rules", Ed. 9.0, 2019.

[6] IEC 60071-2, "Insulation co-ordination - Part 2: Application guidelines", Ed. 4.0, 2018.

[7] IEC 60071-4, "Insulation co-ordination - Part 4: Computational guide to insulation co-ordination and modelling of electrical networks", Ed. 1.0, 2004.

[8] IEEE Standard C57.142-2010, "IEEE Guide to Describe the Occurrence and Mitigation of Switching Transients Induced by Transformers, Switching Device, and System Interaction", April 2011.

[9] E. Bjerkan and H. K. Høidalen, "High frequency FEM-based power transformer modeling: Investigation of internal stresses due to network-initiated overvoltages," in Electric Power Systems Research, vol. 77, Issue 11, pp. 1483-1489, 2007, doi: 10.1016/j.epsr.2006.08.031.

[10] R. C. Degeneff, "A general method for determining resonances in transformer windings," in IEEE Transactions on Power Apparatus and Systems, vol. 96, no. 2, pp. 423-430, 1977, doi: 10.1109/T-PAS.1977.32352.

[11] P. G. Blanken, "A lumped winding model for use in transformer models for circuit simulation," in IEEE Transactions on Power Electronics, vol. 16, no. 3, pp. 445-460, 2001, doi: 10.1109/63.923778.

[12] M. Popov, L. van der Sluis, R. P. P. Smeets and J. L. Roldan, "Analysis of very fast transients in layer-type transformer windings," in IEEE Transactions on Power Delivery, vol. 22, no. 1, pp. 238-247, Jan. 2007, doi: 10.1109/TPWRD.2006.881605.

[13] E. E. Mombello and H. C. Zini, "A novel linear equivalent circuit of a transformer winding considering the frequency-dependence of the impedances," in Electric Power Systems Research, Vol. 77, Issue 8, pp. 885-895, 2007, doi: 10.1016/j.epsr.2006.08.001.

[14] Y. Shibuya, T. Matsumoto, and T. Teranishi, "Modeling and analysis of transformer winding at high frequencies," presented at the Int. Conf. Power Systems Transients, Montreal, Canada, 2005.

[15] J. P. Vieira and L. F. Oliveira, "Behavior of dry-type transformers with respect to resonance and self-mitigation techniques," (in Portuguese), presented at the XXVII National Seminar on Production and Transmission of Electric Energy (SNPTEE 2023), Brasília, Brazil, 2023.

[16] CIGRE TB 901, "High-Frequency Transformer and Reactor Models for Network Studies - Part B: Black-Box Models", JWG A2/C4.52, 2023.

[17] B. Gustavsen, "Study of transformer resonant overvoltages caused by cable-transformer high-frequency interaction," in IEEE Transactions on Power Delivery, vol. 25, no. 2, pp. 770-779, April 2010, doi: 10.1109/TPWRD.2010.2040292.

[18] B. Gustavsen, "Wide band modeling of power transformers," in IEEE Transactions on Power Delivery, vol. 19, no. 1, pp. 414-422, 2004, doi: 10.1109/TPWRD.2003.820197.

[19] B. Gustavsen and B. Tandstad, "Wideband modeling of a 45-MVA generator step-up transformer for network interaction studies," in

Electric Power Systems Research, Vol. 142, pp. 47-57, 2017, doi: 10.1016/j.epsr.2016.08.035.

[20] T. A. Papadopoulos, A. I. Chrysochos, A. I. Nousdilis, and G. K. Papagiannis, “Simplified measurement-based black-box modeling of distribution transformers using transfer functions,” in Electric Power Systems Research, vol. 121, pp. 77-88, 2015, doi: 10.1016/j.epsr.2014.12.003.

[21] B. Gustavsen and A. Semlyen, "Rational approximation of frequency domain responses by vector fitting," in IEEE Transactions on Power Delivery, vol. 14, no. 3, pp. 1052-1061, 1999, doi: 10.1109/61.772353.

[22] B. Gustavsen and H. M. J. De Silva, "Inclusion of rational models in an electromagnetic transients program: Y-parameters, Z-parameters, S-parameters, transfer functions," in IEEE Transactions on Power Delivery, vol. 28, no. 2, pp. 1164-1174, 2013, doi: 10.1109/TPWRD.2013.2247067.

[23] B. Gustavsen and A. Semlyen, "Enforcing passivity for admittance matrices approximated by rational functions," in IEEE Transactions on Power Systems, vol. 16, no. 1, pp. 97-104, 2001, doi: 10.1109/59.910786.

[24] A. O. Soysal, "A method for wide frequency range modeling of power transformers and rotating machines," 1991 IEEE Power Engineering Society Transmission and Distribution Conference, Dallas, USA, 1991, pp. 560-566, doi: 10.1109/TDC.1991.169559.

[25] F. L. Probst, M. V. F. D. Luz, and S. Tenbohlen, "Impact of applied voltage on the frequency response measurements for transient modeling of capacitive voltage transformers," 2024 IEEE International Conference on High Voltage Engineering and Applications (ICHVE), Berlin, Germany, 2024, pp. 1-4, doi: 10.1109/ICHVE61955.2024.10676160.